












# Journal of Experimental Biology and Agricultural Sciences

<http://www.jebas.org>

ISSN No. 2320 – 8694

## Hematite Nanoparticle Mediated Enhancement of *Chlorella minutissima* Lipid Productivity for Sustainable Biodiesel Production

Richa Pahariya<sup>1</sup> , Abhishek Chauhan<sup>2\*</sup> , Anuj Ranjan<sup>2</sup> , Rupesh Kumar Basniwal<sup>3</sup> ,  
 Sumant Upadhyay<sup>4</sup> , Smile Kataria<sup>4</sup> , Hardeep Singh Tuli<sup>5</sup> , Moyad Shahwan<sup>6,7</sup> ,  
 Vinay Mohan Pathak<sup>8</sup> , Tanu Jindal<sup>2\*</sup> 

<sup>1</sup>Amity Institute of Environmental Sciences, Amity University, Noida, U.P., India

<sup>2</sup>Amity Institute of Environmental Toxicology Safety and Management, Amity University, Noida, U.P., India

<sup>3</sup>Amity Institute of Advanced Research and Studies (M&D), Amity University, Noida, U.P., India

<sup>4</sup>Amity Institute of Nanotechnology, Amity University, Noida U.P., India

<sup>5</sup>Department of Biotechnology, Maharishi Markandeshwar (Deemed to be University), Mullana, Ambala 12 133207, Haryana, India

<sup>6</sup>Department of Clinical Sciences, College of Pharmacy and Health Sciences, Ajman University, Ajman 346, United Arab Emirates

<sup>7</sup>Centre of Medical and Bio-Allied Health Sciences Research, Ajman University, Ajman 346, United Arab Emirates

<sup>8</sup>Pritam International Private Ltd, Roorkee, Uttarakhand, India

Received – April 17, 2024; Revision – June 26, 2024; Accepted – July 06, 2024

Available Online – July 15, 2024

DOI: [http://dx.doi.org/10.18006/2024.12\(3\).366.378](http://dx.doi.org/10.18006/2024.12(3).366.378)

### KEYWORDS

Hematite nanoparticles

Microalgal growth

Lipid productivity

Biodiesel production

Iron oxide nanoparticles

Biofuel Enhancement

### ABSTRACT

This study aims to enhance lipid and biofuel productivity from *Chlorella minutissima* with hematite ( $\alpha$ -Fe<sub>2</sub>O<sub>3</sub>) nanoparticles (IONPs) as a growth stimulant. The IONPs were synthesized using chemical method and characterized using X-ray diffraction (XRD), Scanning Electron Microscopy (SEM), and Energy Dispersive X-ray (EDX) analysis to confirm their structure and composition. The experimental setup involved inoculating various concentrations of IONPs (10, 20, and 30 mg·L<sup>-1</sup>) into the microalgal BG-11 growth medium to evaluate their impact on microalgal growth and biodiesel production. Results of this study showed that a concentration of 10 mg·L<sup>-1</sup> of IONPs significantly increased the biomass concentration to 508.1 mg·L<sup>-1</sup> over a 20-day cultivation period, achieving the highest biomass production rate of 31.7 mg·L<sup>-1</sup>·d<sup>-1</sup> at this concentration. The lipid extracted from the microalgal biomass was subsequently transesterified into biodiesel. Key biodiesel properties, such as cetane number, calorific value, density, and viscosity, were measured to assess fuel quality. The findings demonstrate that incorporating hematite nanoparticles into the microalgal growth medium can significantly

\* Corresponding author

E-mail: akchauhan@amity.edu (Abhishek Chauhan), tjindal@amity.edu (Tanu Jindal)

Peer review under responsibility of Journal of Experimental Biology and Agricultural Sciences.

Production and Hosting by Horizon Publisher India [HPI]  
 (<http://www.horizonpublisherindia.in/>).  
 All rights reserved.

All the articles published by [Journal of Experimental Biology and Agricultural Sciences](#) are licensed under a [Creative Commons Attribution-NonCommercial 4.0 International License](#) Based on a work at [www.jebas.org](http://www.jebas.org).



boost both lipid content and overall growth, thereby improving biodiesel production. This study suggests that the use of  $\alpha$ -Fe<sub>2</sub>O<sub>3</sub> nanoparticles presents a promising approach for scalable and sustainable biofuel production from microalgae.

## 1 Introduction

The development of microalgal biomass to produce carbon-neutral and renewable biofuel is essential for environmental sustainability, national economy, and energy security (Vasistha et al. 2021; Zhao et al. 2024a). Biodiesel, which is classified as an alkyl monoester of long-chain fatty acids, is a sustainable fuel that is extensively utilized in diesel engines across several nations (Yaşar 2020; Moschona et al. 2024). It has been proposed that biofuels such as biodiesel and bioethanol present captivating alternatives to renewable energy sources. Microalgae have been thoroughly investigated as a source for generating biofuels. The main components present in microalgal biomass are lipids, proteins, and polysaccharides. The lipid component is used as the primary material for biodiesel production. Some oleaginous species such as *Chlorella* (Saxena et al. 2020), *Nitzschia* (Huang et al. 2022), and *Scenedesmus obliquus* (He et al. 2017) are the most widely researched species in biodiesel production (Ma et al. 2022). The intensive part of producing biofuel from microalgae is extracting biomass from the diluted culture broth (Muhammad et al. 2021). Consequently, one of the main obstacles to the commercialization and large-scale production of microalgae is the low cell concentration and lipid content. Thus, the methods to enhance the growth of microalgae with comparatively greater biomass concentration and lipid accumulations are significant requirements in biofuel production (Kaushik et al. 2009; Ganesh Saratale et al. 2022). Adding nanoparticles throughout the cultivation and harvesting phases is one of the many methods that may be employed to improve microalgae development (Vasistha et al. 2021). The application of NPs during the microalgal growth phase can increase the amount of CO<sub>2</sub> that is absorbed from the atmosphere and even improve the photobioreactor's ability to convert light efficiently, which accelerates the growth of the microalgae (Pahariya et al. 2023). While incorporating nano-additives into microalgae cultures, it is important to consider both the characteristics and concentration of the NPs carefully. However, the impact of NPs on the growth and biochemical composition of microalgae depends closely on their unique physical characteristics (Saxena et al. 2020). It is reported that the lipid content of *Chlorella fusca* LEB 111 increased by 10.9% and 16.7% when grown outdoors with 0.3 and 0.5 g L<sup>-1</sup> of nanofibers, respectively. These nanofibers are composed of polymeric nanofibers (10% w/v) made from polyacrylonitrile (PAN) dissolved in dimethylformamide (DMF) with the addition of 4% (w/v) Fe<sub>2</sub>O<sub>3</sub>NPs. When exposed to uncoated nano-zero-valent iron (nZVI), *Tetraselmis suecica* showed a lipid augmentation of 41.90% in the study on the effects of nZVI on various microalgae species. Additionally, they noticed that adding inorganically coated nZVI powder to *Pavlova lutheri* resulted in a 46.34% increase in

lipid levels (Kadar et al. 2012). The biodiesel yield in *Spirulina* was enhanced up to 81% by Fe<sub>2</sub>O<sub>3</sub> nanoparticles, which were synthesized using a green procedure involving extracts from *Hibiscus rosa-sinensis* (Banerjee et al. 2019). Similarly, it was found that the addition of a 100 mg. L<sup>-1</sup> dose of nZVI enhances the biomass concentration in *Isochrysis galbana* by 18.75%, accompanied by a 3.57% increase in lipid accumulation (Kadar et al. 2012). Similarly, the lipid content was increased by 16.7% in *Chlorella fusca* when nZVI was added at 0.5 g L<sup>-1</sup> (Da Silva Vaz et al. 2020). The impact of nanoparticles on the growth and biochemical composition of microalgae is contingent upon their physical characteristics (Khan et al. 2018). *Candida rugosa* lipase was employed for the transesterification of algal lipids after being immobilized on graphene oxides magnetized with NiFe<sub>2</sub>O<sub>4</sub> nanoparticles (NiFe<sub>2</sub>O<sub>4</sub>-GO). This nanocomposite proved to be an outstanding nano biocatalyst for efficient biodiesel generation, with biodiesel production efficiency three times better than that of free enzymes (Aghabeigi et al. 2023). The increase in lipid content is attributed to the use of NPs, which positively impact cellular activity. For example, iron (Fe) serves as a crucial micronutrient for microalgae, playing a vital role in essential cellular functions such as photosynthesis and respiration. The availability of iron regulates their productivity, community structure, and overall ecosystem functioning (Cheng et al. 2020). In contrast, Fe<sub>2</sub>O<sub>3</sub> nanoparticles showed toxicity towards *C. sorokiniana* even at the low dose of 2 mg. L<sup>-1</sup>, whereas the dose of 20 and 30 mg. L<sup>-1</sup> in *C. pyrenoidosa* increased biomass productivity and lipid content (Rana et al. 2020). The effects of copper and selenium nano aqua chelate carboxylated with citric acid on biomass accumulation in *C. vulgaris* were also investigated. The inoculation of 0.67–4 mg. L<sup>-1</sup> of Cu nano carboxylates resulted in an approximately 20% increase in *Chlorella* biomass. However, concentrations of 20–40 mg. L<sup>-1</sup> significantly inhibited algal development after the 12<sup>th</sup> day of incubation. Se nanocarboxylates at concentrations of 0.4–4 mg. L<sup>-1</sup> also fostered the growth of *C. vulgaris*, leading to a 40–45% rise in biomass (Mykhaylenko and Zolotareva 2017).

Previous research has shown that NPs concentration can significantly impact microalgae growth; the specific effects vary depending on several factors. Such factors include the type of NPs, the microalgae species itself, and environmental conditions like culture media and pH. Among microalgae, *C. minutissima* is a particularly promising strain for biofuel production. It is also known to be less sensitive to Fe NPs compared to other types, such as nZVI and Fe<sub>3</sub>O<sub>4</sub>. However, the impact of IONPs on *C. minutissima*'s growth and its potential for biofuel production remains unclear.

Therefore, the present research aims to investigate the effect of IONPs on both the growth and lipid accumulation of *C. minutissima*. It involved testing various concentrations of IONPs in BG11 media and measuring parameters like cell density and lipid accumulation within *C. minutissima*. By examining these factors, this research will provide valuable insights into the potential use of IONPs in *C. minutissima* cultivation for biofuel production. The findings will help us understand if specific IONPs concentrations can promote both microalgae growth and lipid accumulation, making them a viable tool for this purpose.

## 2 Materials and Methods

### 2.1 Microalgal species

The oleaginous microalga *C. minutissima* MCC 27 was obtained from the Centre for Blue Green Algae, Indian Agricultural Research Institute (IARI), New Delhi, India. A sterile culture BG 11 medium was prepared for the inoculation, and pH was maintained at 7.1.

### 2.2 Chemical synthesis of Fe<sub>2</sub>O<sub>3</sub> nanoparticles

IONPs termed "Hematite" were synthesized using the sol-gel process as per the method described by Paulson and Jothibas (2021). In the experiment, 100 mL of distilled water was used to dissolve the 0.3 M of Ferric chloride hexahydrate, which was maintained by vigorous stirring at 300 rpm for 15 minutes. Following that, a reagent solution made up of 10 mL of NH<sub>3</sub>-ammonia solution and 10 mL of distilled water was combined. The produced reagent solution was then carefully added to the ferric chloride anhydrous solution, and it was stirred vigorously (400 ± 20 rpm) for one hour at 80 °C. The gel was put into a petri dish once the initial cleaning was finished and kept in the oven at 80 °C for 24 hours. The resultant nano-powder sample was then stored for subsequent characterizations after being calcined at 400 °C for 3 hours in an open environment.

### 2.3 Materials Characterization

#### 2.3.1 X-ray diffraction (XRD)

The X-ray diffraction was performed using a Philips XRD 3100 diffractometer (Philips Electronics Co., Eindhoven, Netherlands) with a medium scan rate of 0.3 degrees per second over a 2θ range of 20-70°.

#### 2.3.2 Scanning Electron Microscopy (SEM)

The SEM and EDX study was performed using TESCAN Magna 200 eV-30 KV along with cross-sectional, morphology, and elemental analysis for Fe & O.

### 2.4 Evaluation of microalgal growth

Initial studies were carried out in 250 mL Erlenmeyer flasks with 100 mL of BG 11 medium to examine the biomass potential and growth profiles. 10% (v/v) of freshly grown *C. minutissima* was added to the medium containing flasks and incubated in a microalgae growth chamber at 25 ± 2 °C. All the experiments were carried out in triplicates. The flasks were kept under LED light (about 2500 Lux) for an 18:6 light and dark period (18-hour light-dark cycle 6 hours) for 20 days. Throughout 20 days, the optical density of the microalgae was measured at 680 nm utilizing an Agilent Technologies Cary 60 UV-Vis Spectrophotometer.

To measure the effect of iron nanoparticles, *C. minutissima* was cultured in 100 mL of BG11 media supplemented with different concentrations of nanoparticles (0, 10, 20, and 30 mg·L<sup>-1</sup>). The cultures were maintained under the controlled conditions mentioned above. The growth of the microalgae was measured by sampling the culture every two days for 20 days. After 20 days, the microalgal biomass was harvested by centrifugation and washed with double distilled water to remove impurities. After centrifugation, the pellets were dried in an oven at 60 °C until they reached a consistent weight. After drying, the biomass was placed in desiccators to estimate the accumulation of lipids and biodiesel. Biomass concentration, biomass yield, and biomass productivity were calculated using corresponding equations (1), (2), and (3).

$$\text{Biomass concentration} = \text{Weight (mg)} / \text{volume of culture (L)} \quad (1)$$

$$B = X_f - X_0 \quad (2)$$

Where B= biomass yield (g·L<sup>-1</sup>)

X<sub>f</sub>= final biomass concentration

X<sub>0</sub> = initial biomass concentration

$$P_b = (X_2 - X_1) / (t_1 - t_0) \quad (3)$$

Where P<sub>0</sub>= biomass productivity

X<sub>2</sub> and X<sub>1</sub>= biomass concentrations

### 2.5 Calculation of Chlorophyll a

Chlorophyll-a (chl-a) was estimated using the colorimetry method (Porra et al. 1989). In summary, a 1.5 mL Eppendorf tube containing an aliquot (1 mL) of microalgae culture was centrifuged at room temperature for 10 minutes at 6000 rpm. The sample was then rinsed three times with deionized water to remove the impurities. The pellets were again suspended in 1 millilitre of methanol after the supernatant was disposed off. The tubes were tightly sealed with parafilm and immersed in a water bath heated to

60 °C for 30 minutes to extract chlorophyll-a. Following cooling to room temperature, absorbance readings were taken at wavelengths of 652 nm, 665.2 nm, and 750 nm. Porra's equation was then used to estimate the concentration of chl-a in  $\mu\text{g}\cdot\text{mL}^{-1}$ .

$$\text{Chl - a} = 16.29 (A_{665.2} - A_{750}) - 8.54 (A_{652} - A_{750}) \quad (4)$$

## 2.6 Lipid extraction from harvested microalgae

The lipids from microalgae were extracted using the modified Bligh and Dyer (1959) method. Then, dried and powdered microalgal biomass was dispersed in distilled water. After microwaving at 540 W, the microalgal cells were disrupted, and the suspension was allowed to cool to room temperature. Subsequently, chloroform and methanol were introduced into the microalgal suspension. The mixture was vigorously shaken manually and left at room temperature for 4 hours. Following this, water was added to aid in the separation of phases. The mixture was subsequently left undisturbed until the organic layer settled and the upper phase became clear (Lee et al. 2010). The organic phase, containing chloroform and lipids, was carefully extracted, and its volume was recorded, and the lipid content was calculated using the following equation:

$$\text{Lipid content (\%)} = \frac{\text{Mass of lipid (in grams)} \times 100}{\text{Mass of algae culture (in grams)}}$$

## 2.7 Fatty Acid Methyl Ester (FAME) formation

FAME formation was carried out by Transesterification (Mishra et al. 2014). Briefly, in this process, methanol was added to sodium hydroxide into the glass blender. The mixture of methanol and sodium hydroxide was appropriately mixed with the help of a magnetic stirrer after dissolving NaOH in methanol. Then, the extracted oil was transferred into a glass blender for 30 minutes.

Following that, the mixture was put into a sterile container. The mixture is divided into two layers after two to three hours. The first layer was biodiesel, and the second was glycerine. The biodiesel was then washed multiple times with distilled water to remove traces of alcohol, catalyst and glycerol.

### 2.7.1 FT-IR Analysis

A Bruker Vertex 70 FTIR spectrophotometer with a Platinum ATR (attenuated total reflection) module was used to conduct the spectral study. FT-IR spectra were produced at 400–4000  $\text{cm}^{-1}$  (Portaccio et al. 2023). The Origin software (version 5.0, 2007) was then used to evaluate these spectra.

## 2.8 Assessment of biodiesel fuel properties

The biodiesel obtained from *C. minutissima* grown in BG 11 was subjected to testing for its physical characteristics, including specific density (Prabakaran et al. 2021), viscosity (Al-Ansari et al. 2023), calorific value (Boopathi et al. 2023), cetane number (Tesfa et al. 2013), iodine value, and oxidative stability (Geng et al. 2023). These tests were conducted according to the protocols outlined by ASTM D6751 and EN 14214 fuel standards.

## 3 Results

### 3.1 Morphology of *C. minutissima*

Under the scanning microscope, *C. minutissima* has a unicellular structure, yellow-green color, and a spherical shape with a diameter ranging from 5 to 15  $\mu\text{m}$ . The cells appear spherical or ellipsoidal under a scanning electron microscope, and their walls either have smooth surfaces or uneven coastal portions, as shown in Figure 1. The cells exist in either a unicellular state or in the palmella stage.

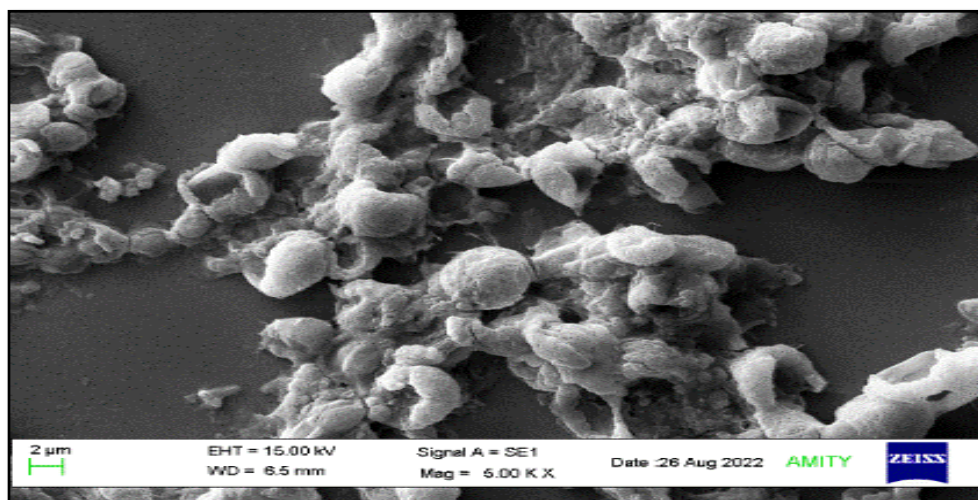


Figure 1 Scanning microscopic image of *C. minutissima*

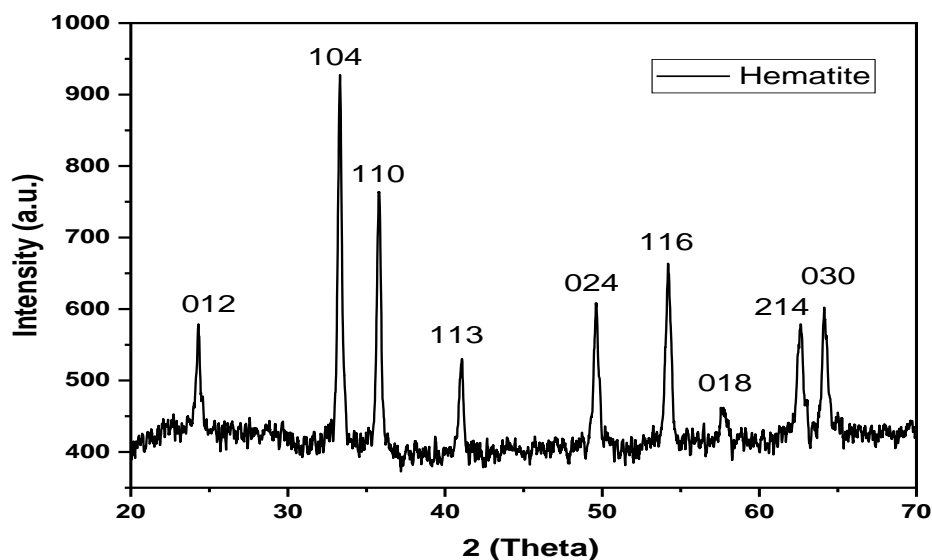


Figure 2 X-ray diffraction (XRD) pattern of synthesized nanoparticles of iron oxide ( $\alpha$ - $\text{Fe}_2\text{O}_3$ )

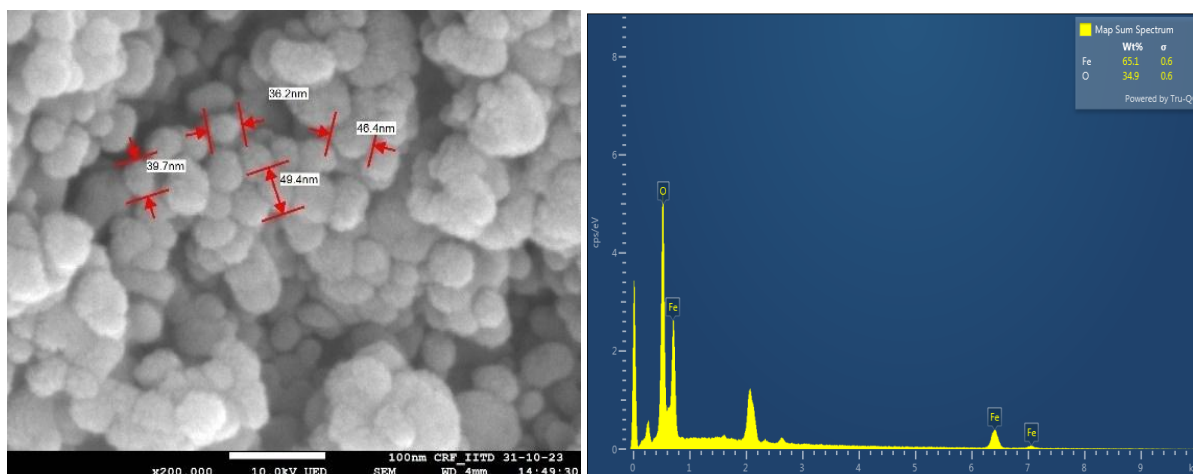


Figure 3 (a) SEM (b) EDX image of synthesized  $\text{Fe}_2\text{O}_3$  ( $\alpha$ - $\text{Fe}_2\text{O}_3$ ) nanoparticles

### 3.2 XRD analysis

Figure 2 shows the X-ray diffraction pattern for iron oxide ( $\alpha$ - $\text{Fe}_2\text{O}_3$ ). The X-ray diffraction study for  $\alpha$ - $\text{Fe}_2\text{O}_3$  shows the characteristic peaks for the 104 plane corresponding to the  $2\theta$  angle of 33.29, implying the formation of  $\alpha$ - $\text{Fe}_2\text{O}_3$ . The referred X-ray diffractions are from the JCPDS Card No. 86-0550. The crystallite size was determined using the Debye-Scherrer's equation:  $D = K\lambda / \beta \cos\theta$

Where the wavelength of Cu-K $\alpha$  radiation utilized is  $\lambda = 1.5418 \text{ \AA}$ , the form factor is  $k = 0.9$ , the full-width half maximum (FWHM) is expressed in radians ( $\beta$ ), the crystallite's diameter is  $D$ , and Bragg's angle is  $\theta$  (Sun et al. 2006). The crystallite size for the  $\alpha$ - $\text{Fe}_2\text{O}_3$  was calculated to be 40 nm from FWHM of the most intense (104) diffraction peak using Debye-Scherrer's equation.

### 3.3 SEM analysis

Figure 3 (a, b) shows the FE-SEM micrograph for the  $\alpha$ - $\text{Fe}_2\text{O}_3$  at a scale of 100nm, along with the elemental X-ray electron energy and their elemental mapping. The particle size calculated for sample  $\alpha$ - $\text{Fe}_2\text{O}_3$  was  $\sim 46 \text{ nm}$  using SEM, which is in good agreement with the size calculated using XRD data.

### 3.4 Assessment of growth parameters in *C. minutissima*

*C. minutissima* is the fastest-growing strain. After 20 days of incubation, microalgal cells were subjected to further analysis. To access the growth parameters, the strain was cultured in a BG 11 medium. Figure 4 shows that the OD of samples increased and reached the maximum in 14 days. The absorbance ( $A_{680}$ ) of the culture microalgae strain was recorded using a spectrophotometer



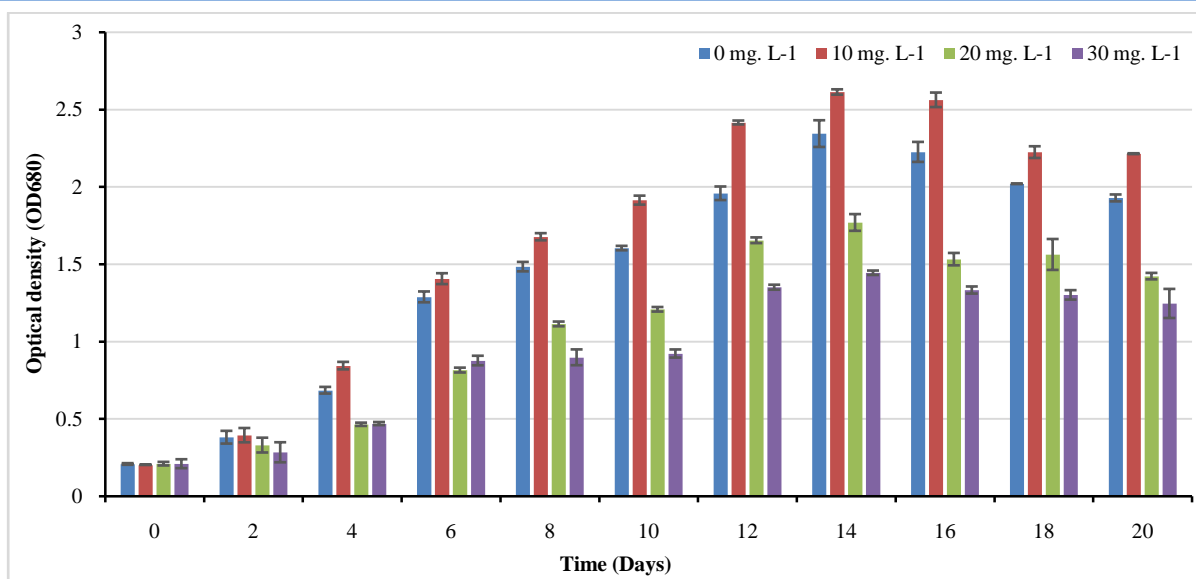


Figure 4 Graphical representation of optical density on various IONPs concentrations on *C. minutissima*

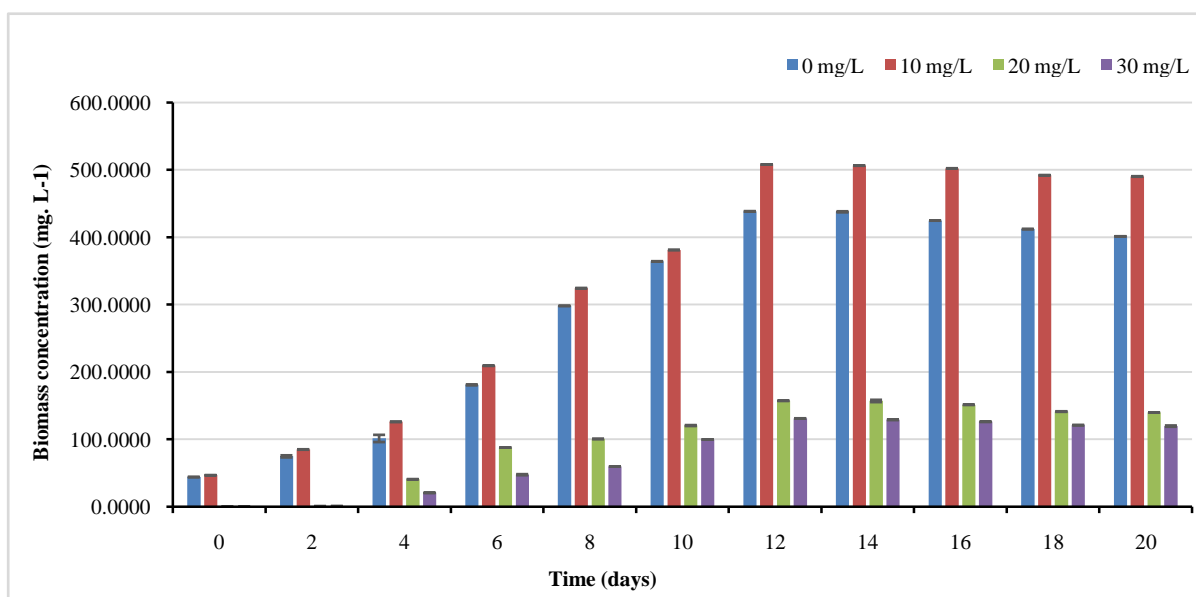


Figure 5 Graphical representation of biomass concentration on various IONPs concentration on *C. minutissima*

(Agilent Technologies Cary 60 UV-Vis). According to Figure 4, the optical density is at 0 mg L<sup>-1</sup> observed 2.34 for *C. minutissima*. Further, the highest *C. minutissima* optical density of  $2.61 \pm 0.08$  was exhibited at a 10 mg L<sup>-1</sup> IONPs dose, while 20 and 30 mg L<sup>-1</sup> showed  $1.76 \pm 0.05$  and  $1.44 \pm 0.01$  on 14<sup>th</sup> day of inoculation respectively (Figure 4).

### 3.4.1 Estimation of biomass concentration on *C. minutissima*

After 20 days of the batch study, a gradual exponential growth phase extended until the 14<sup>th</sup> day (Figure 5). Biomass concentration was calculated based on the dry cell weight (DCW).

The highest biomass concentration ( $438.533 \pm 0.35$  mg L<sup>-1</sup>) was reported for the control sample (0 mg L<sup>-1</sup>).

### 3.4.2 Estimation of biomass concentration on *C. minutissima* on different concentrations of synthesized Fe<sub>2</sub>O<sub>3</sub>

The growth pattern of biomass for *C. minutissima* is illustrated in Figure 5. Until the 8<sup>th</sup> day, there were no significant changes reported in various concentrations of IONPs in the culture medium, and the highest concentration of 508.1 mg L<sup>-1</sup> was reported in 10 mg L<sup>-1</sup>. Whereas 157.53 and 131.3 mg L<sup>-1</sup> recorded in 20 and 30 mg L<sup>-1</sup> dose of IONPs

### 3.4.3 Estimation of Chlorophyll-a in *C. minutissima*

During the growth, chlorophyll-a content also increased in correspondence to optical density. The results of the study revealed a concentration of  $12.00 \pm 0.5689 \mu\text{g}\cdot\text{mL}^{-1}$  Chlorophyll-a in *C. minutissima* up to the 12<sup>th</sup> day. However, after the 12<sup>th</sup> day, chlorophyll-a concentration starts decreasing gradually (Figure 6).

### 3.4.4 Estimation of Chlorophyll-a in *C. minutissima* on different concentrations of synthesized $\text{Fe}_2\text{O}_3$

Exposure to various concentrations of IONPs ranging from 10 to 30  $\text{mg L}^{-1}$  resulted in different levels of Chlorophyll-a in *C. minutissima* cultures (Figure 6). Further, Chlorophyll-a concentration was higher ( $17.11 \pm 1.29 \mu\text{g}\cdot\text{mL}^{-1}$ ) at 10  $\text{mg L}^{-1}$  IONPs dose until the 12<sup>th</sup> day of cultivation while at 30 and 20  $\text{mg L}^{-1}$  dose of IONPs chl-a concentrations were 6.3 and 9.073

$\mu\text{g}\cdot\text{mL}^{-1}$ , respectively. However, impairment in chl-a concentration was noted at all IONPs doses starting on the 14<sup>th</sup> day.

### 3.4.5 Estimation of biomass productivity and yield on *C. minutissima*

Once inoculated into BG 11 media, *C. minutissima* exhibited exponential growth. The biomass productivity at 0  $\text{mg L}^{-1}$  was recorded  $26.66 \text{ mg}\cdot\text{L}^{-1}\cdot\text{d}^{-1}$  and the final biomass yield was recorded  $357.003 \text{ mg}\cdot\text{L}^{-1}$

### 3.4.6 Estimation of biomass productivity and yield on *C. minutissima* on different concentrations of synthesized $\text{Fe}_2\text{O}_3$

As shown in Figure 7, biomass productivity was recorded  $31.74 \text{ mg}\cdot\text{L}^{-1}\cdot\text{d}^{-1}$  at 10  $\text{mg L}^{-1}$  while 9.69 and 8.1  $\text{mg}\cdot\text{L}^{-1}\cdot\text{d}^{-1}$  was observed at 20 and 30  $\text{mg L}^{-1}$ , respectively. Similarly, At 10  $\text{mg}\cdot\text{L}^{-1}$  IONPs

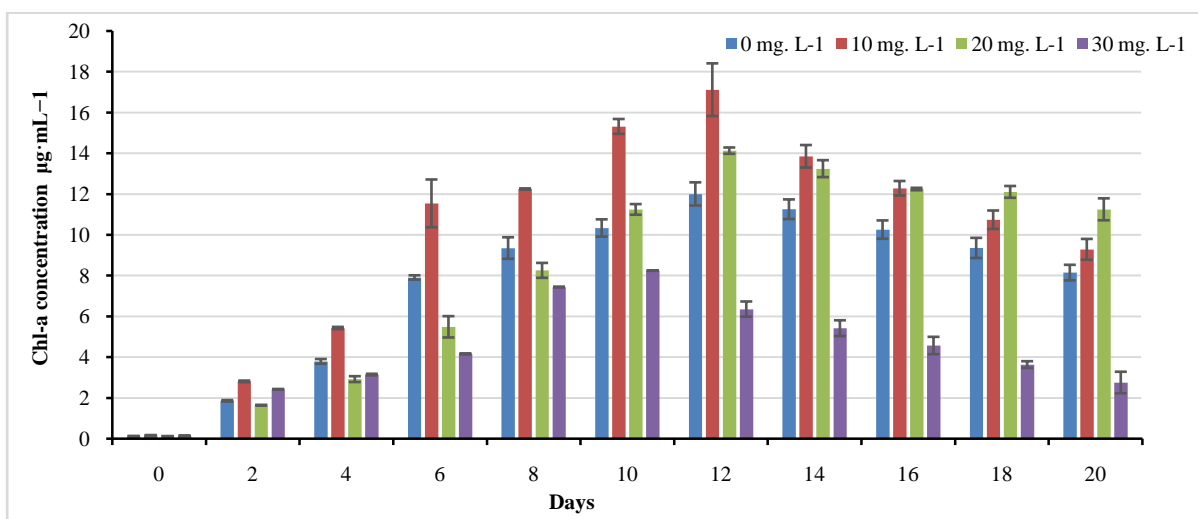


Figure 6 Graphical representation of Chl-a on various IONPs concentration on *C. minutissima*

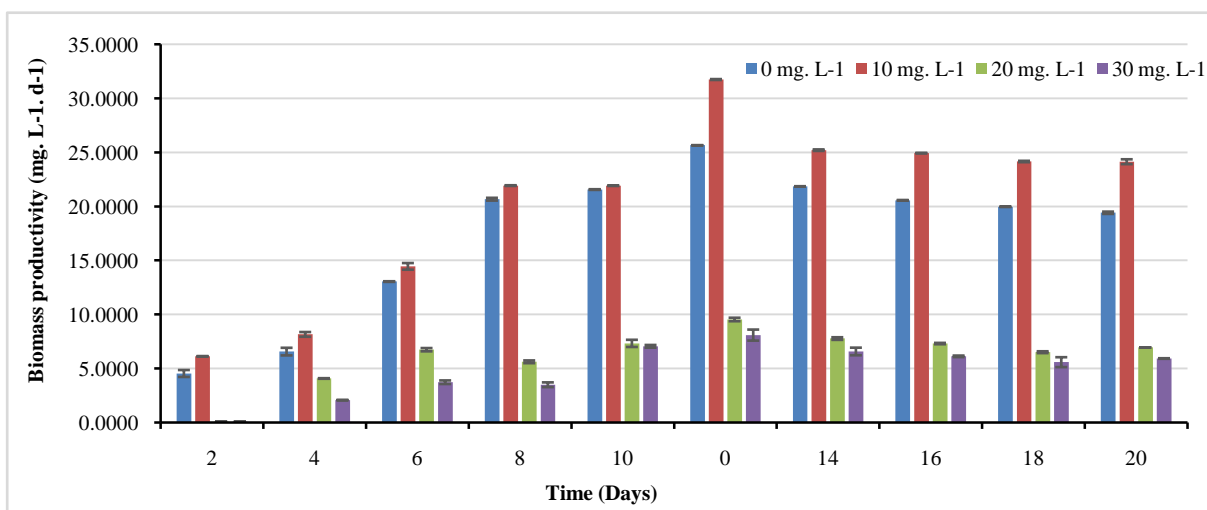


Figure 7 Graphical representation of biomass productivity on various IONPs concentrations on *C. minutissima*

dose, *C. minutissima* demonstrated the highest biomass yield of 443.167 mg.L<sup>-1</sup>, whereas at 20 mg.L<sup>-1</sup> and 30 mg.L<sup>-1</sup>, the yields were 139.86 mg.L<sup>-1</sup> and 119.75 mg.L<sup>-1</sup>, respectively. At 10 mg.L<sup>-1</sup> biomass yield is 24% higher in comparison to other doses.

### 3.5 Lipid productivity

In this study, the assessment of the total lipid content or productivity of *C. minutissima* was conducted following the harvesting process. Among the different doses of IONPs, the highest lipid production (29.52%) was reported at 10 mg.L<sup>-1</sup>, which was 28.52 % higher than control. The observed changes in growth and lipid production suggest the absorption of NPs and their potential effects. This phenomenon is intricately linked to the specific nanoparticles used and the choice of microalgal strain. The interaction between these factors plays a crucial role in shaping the outcomes, emphasizing the need for a detailed understanding of the interplay between IONPs, nanoparticles, and microalgal strains to optimize and tailor the effects for desired outcomes in applications such as biomass and lipid production.

#### 3.5.1 FTIR

The FTIR spectra of the microalgal oil are displayed in Figure 8. The region indicates the presence of lipids in the sample in

the spectra between 3100 and 2800 cm<sup>-1</sup>, which arises due to the vibrations of both symmetric and asymmetric stretching of the -CH<sub>2</sub>- groups. These -CH<sub>2</sub>- groups serve as the foundational structure of lipids and demonstrate absorption, especially at 2923 and 2865 cm<sup>-1</sup>. The algal oil's FTIR spectra revealed well-absorbed areas between 3500 and 3000 cm<sup>-1</sup>, 1747 and 1172 cm<sup>-1</sup>, and 800 and 700 cm<sup>-1</sup>. The regular peaks at 2923 and 2860 cm<sup>-1</sup> result from the -CH<sub>2</sub>- groups' symmetric and asymmetric stretching vibrations. The spectra of algal oil also showed peaks at 3005 cm<sup>-1</sup> from double bond stretching and 1300–1100 cm<sup>-1</sup> from the C–O bond (axial stretching). There were also observed absorption peaks at 722 cm<sup>-1</sup> attributed to the -CH<sub>2</sub>- bending out of the plane and at 1365–1377 and 1465 cm<sup>-1</sup> attributed to the -CH<sub>3</sub> bond. The existence of these peaks signifies the transformation of oil into biodiesel.

Table 1 compiles the different fuel qualities of *C. minutissima* biodiesel produced under ideal circumstances. The biodiesel showed a density of 0.86 g/cm<sup>3</sup>, a viscosity of 3.24 mm<sup>2</sup>/s and an iodine value of 124 g I<sub>2</sub>/100 g, which abided by the fuel standards. All the tested parameters were found to be closely aligned with the American Society for Testing and Materials (ASTM) D6751 and EN 14214 fuel standards, respectively.

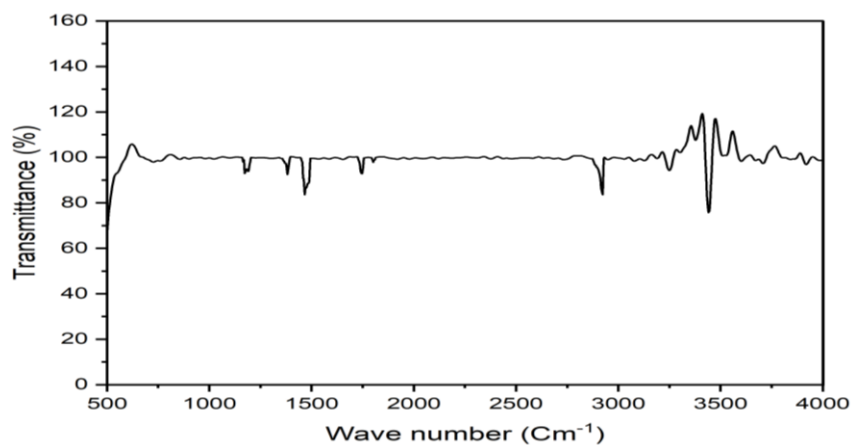


Figure 8 FTIR spectrum of *C. minutissima* algal oil

Table 1 Comparison of *C. minutissima* biodiesel with various biodiesel standards

Parameters	Present study	ASTM standards	EN 14214
Density (g cm <sup>-3</sup> )	0.86	-	0.86-0.90
Viscosity (mm <sup>2</sup> /s)	3.5	1.9-6.0	3.5-5.0
Calorific value (MJ Kg <sup>-1</sup> )	35.58	-	-
Iodine value (g I <sub>2</sub> /100 g)	124	-	<120
Cetane number	50.34	>47	>51
Degree of unsaturation (%)	70.15	-	-
Oxidative stability	6	-	>6



#### 4 Discussion

Fe<sub>2</sub>O<sub>3</sub> nanoparticles were chosen for the microalgae due to their demonstrated highest efficiency in harvesting in this research. Surface characterization was analyzed through XRD, as depicted in Figure 2. The pattern in the figure indicates the crystalline nature of Fe<sub>2</sub>O<sub>3</sub> nanoparticles. The observed peaks are corresponding to pure Fe<sub>2</sub>O<sub>3</sub> nanoparticles. The presence of narrow and sharp peaks suggests that the hematite products exhibit high crystallinity (Lassoued et al. 2017). The average grain size of the synthesized  $\alpha$ -Fe<sub>2</sub>O<sub>3</sub> was determined by SEM to be less than 100 nm. SEM analysis of the synthesized nanoparticles revealed the formation of spherical particles in shape and uniform distribution (Qayoom et al. 2020). Additionally, the elemental composition of Fe<sub>2</sub>O<sub>3</sub> nanoparticles was examined through energy dispersive spectroscopy, as depicted in Figure 3(b). The analysis revealed the presence of peaks corresponding to Fe and O, indicating the absence of impurities.

The addition of IONPs demonstrated positive outcomes regarding the growth, biomass concentration, biomass productivity and biomass yield of *C. minutissima*. According to the current findings, *C. minutissima* and NPs doses of 10, 20, and 30 mg·L<sup>-1</sup> were chosen for subsequent investigations and the growth of *C. minutissima* was analyzed at OD<sub>680</sub>. A similar result was reported by Attre et al. (2018), who cultured *C. minutissima* strain on glycine medium. Overall, the highest biomass concentration of 508.1 mg·L<sup>-1</sup> was achieved at 10 mg·L<sup>-1</sup>. In contrast, biomass concentrations for NPs doses of 20 and 30 mg·L<sup>-1</sup> were recorded as 157.33 ± 0.32 and 131.3 ± 0.26 mg·L<sup>-1</sup>, respectively. It was noted that in the low-concentration range of nanoparticles, the biomass of algal cells initially increased but then declined with higher concentrations of Fe<sub>3</sub>O<sub>4</sub> NPs (Wang et al. 2021). Results of Kaliampurthi et al. (2019) are contradictory to the findings of the present study, where no aggregation was reported at a lower concentration of 50 mg·L<sup>-1</sup> for ZnO nanoparticles, but higher microalgae accumulation was noted at 100 mg·L<sup>-1</sup> (Kaliampurthi et al. 2019). Further, carbon nanotubes inhibit cell growth in freshwater microalgae *Scenedesmus obliquus*, while nano Fe<sub>2</sub>O<sub>3</sub> promotes growth in the same species (He et al. 2017). Up to the 14<sup>th</sup> day, there was a notable distinction in biomass productivity among various doses of NPs. In the current study, biomass productivity is measured in the NP-treated samples, and higher biomass (31.74 mg·L<sup>-1</sup>·d<sup>-1</sup>) was observed at 10 mg·L<sup>-1</sup> IONPs, while at higher concentrations, it decreased. The biomass productivity, in the context of using MIL-100(Fe), a type of metal-organic framework incorporating iron, was measured in *Arthrospira* sp., and it was determined to be 0.61 g·L<sup>-1</sup> (Cheng et al. 2020). Biomass yield was 24.12% at 10 mg·L<sup>-1</sup>, which is higher than that of the control. The stimulation of algal proliferation may be linked to the dissociation of minute iron nanoparticles (Marsalek et al. 2012). Due to its association with the

photosynthetic electron transport chain, iron may be required for both growth and metabolic alterations, as suggested by the enhanced growth of microalgal biomass; this supports the hypothesis. However, the rise in NPs concentrations is adversely correlated with the notable reduction in growth. The growth of marine phytoplankton *Skeletonema costatum* and *Nitzschia closterium* is inhibited by metal salt (Cu<sup>2+</sup>), nano-metal (nano-Cu), and nano-metal oxide (nano-CuO). Cu<sup>2+</sup> and nano-Cu EC50 values, which range from 0.356 to 0.991 mg·L<sup>-1</sup> and 0.663 to 2.455 mg·L<sup>-1</sup>, have been shown to have an impact on the extracellular polymeric compounds and amino acids secreted by *S. costatum* and *N. closterium* microalgae (Huang et al. 2022). Further, Chl-a concentrations also decreased at all IONPs doses starting on the 14<sup>th</sup> day. The highest chl-a was recorded (17.11 ± 0.09 µg·mL<sup>-1</sup>) at 10 mg·L<sup>-1</sup>. Moreover, the concentration of 30 mg·L<sup>-1</sup> exhibited the lowest number of Chl-a. Studies have indicated that titanium oxide nanoparticles notably hindered the growth and biomass (including dry weight, chlorophyll A, and total chlorophyll) of *Chlorella vulgaris* due to their surface adsorption on the algal cell, which promotes growth inhibition (Roy et al. 2018). On the contrary, when Fe<sub>2</sub>WO<sub>6</sub> NPs inoculated at different concentrations in the culture medium of *Dunaliella salina*, the cell density, chlorophyll a and b, increased at lower 20 ppm concentrations (Hassanpour et al. 2020).

As per a recent study, in *Scenedesmus obliquus*, lower concentrations of CNTs and Fe<sub>2</sub>O<sub>3</sub> increased the chlorophyll content, while higher concentrations repressed photosynthesis (He et al. 2017). Iron is essential for photosynthesis, cell respiration, and the creation of phytohormones and chlorophyll (Zhao et al. 2024b). From the current observations, it was hypothesized that the lower dose of NPs functions as a source of iron for the growth of microalgae. In general, NPs demonstrated favourable effects on *C. minutissima*, leading to increased biomass growth and chlorophyll-a concentration at 10 mg·L<sup>-1</sup> NPs dose. In contrast, recent research signifies a significant advancement in the field. Cultivation of *C. minutissima* not only remained viable but also demonstrated an enhanced growth rate in NP-supplemented media. This opens up new possibilities for employing NPs in large-scale cultivation of targeted microalgae, leading to increased biomass production. The highest lipid production of 29.52% was observed at 10 mg·L<sup>-1</sup> NPs dose, which was 28.52 % higher than that of control (15.98%). The change in growth and lipid production is a sign of metal oxide absorption and its consequences. Using Carbon Nano Tubes, Fe<sub>2</sub>O<sub>3</sub>, and MgO nanoparticles, increases in lipid production were reported at 8.9%, 39.6%, and 18.5%, respectively (He et al. 2017). The treatment with 50 mg/L of ZnO-NP increased the synthesis of neutral lipids (6.08-fold) and triacylglycerol (8.21-fold) without causing complete growth inhibition (Kaliampurthi et al. 2019). The rise in lipid synthesis indicates a change in cellular metabolism. Likewise, Chandra et al. (2019) observed 37.24 mg·L<sup>-1</sup>·d<sup>-1</sup> a lipid content in *C.*

*minutissima* at a concentration of 50 mg. L<sup>-1</sup>. In contrast, a slight decrease in lipid (23.07 %) was also observed at NPs doses of 20 mg.L<sup>-1</sup>. At this concentration, the relatively low lipid percentage partially suggests the absorption of NPs and the generation of reactive oxygen species (Shi et al. 2017). Hence, the gradual uptake of NPs at an optimal dose could help balance oxidative stress and enhance lipid productivity. Previous research indicates that in cultures containing NPs, microalgal biomass typically has only a few nanoparticles adhering to the cell surface (Taghizadeh et al. 2022). Nanomaterials can stimulate the generation of reactive oxygen species (ROS), initiating the cellular mechanism of oxidative stress (Wang et al. 2021). However, a significant decline in biomass growth represents a considerable constraint in conditions of nutrient scarcity. However, the NPs that were examined for this study did not exhibit any restrictions on the growth of microalgae. Overall, 10 mg. L<sup>-1</sup> NPs dose was shown to be optimal for *C. minutissima* development and growth with improved lipid accumulation based on the acquired biomass potential and lipid yields. The region indicates the presence of lipids in the sample in the spectra between 3100 and 2800 cm<sup>-1</sup>, which is caused by the symmetric and asymmetric stretching vibrations of the symmetric CH<sub>2</sub> and asymmetric CH<sub>3</sub> and CH<sub>2</sub> stretching (Wallach et al. 1979). These -CH<sub>2</sub>- groups serve as the lipids' structural backbone and exhibit absorption, especially at 2923 and 2865 cm<sup>-1</sup> (Portaccio et al. 2023). The algal oil's FTIR spectra revealed well-absorbed areas between 3500 and 3000 cm<sup>-1</sup>, 1747 and 1172 cm<sup>-1</sup>, and 800 and 700 cm<sup>-1</sup>. The normal peaks at 2923 and 2860 cm<sup>-1</sup> result from the -CH<sub>2</sub>- groups' symmetric and asymmetric stretching vibrations (Arif et al. 2021). The spectra of algal oil also showed peaks at 3005 cm<sup>-1</sup> from double bond stretching and 1300–1100 cm<sup>-1</sup> from the C–O bond (axial stretching). There were also observed absorption peaks at 722 cm<sup>-1</sup> attributed to the -CH<sub>2</sub>- bending out of the plane and at 1365–1377 and 1465 cm<sup>-1</sup> attributed to the -CH<sub>3</sub> bond (Nematian et al. 2020). The existence of these peaks signifies the transformation of oil into biodiesel. The characteristics of biodiesel predominantly depend on its fatty acid esters (Mondal et al. 2021). In a study, Mallick et al. (2012) found that the calorific value of *C. minutissima* is comparable to *C. vulgaris*. Further, the Iodine value in *C. minutissima* shows a high oxidative value, which means the presence of a mixture of fatty acids; it is found within the range according to ASTM and EN 14214 (Thiruganasambandham 2018). Density plays a significant role in airless combustion systems as it directly impacts the efficiency of fuel atomization. Density was recorded at 0.86 g cm<sup>-3</sup> in *C. minutissima*, which is also in synchronization with ASTM and EN standards. The above results show that *C. minutissima* fuel properties are aligned well with commercial biodiesel.

## Conclusion

The utilization of hematite (α-Fe<sub>2</sub>O<sub>3</sub>) nanoparticles demonstrates a promising approach to enhance lipid and biofuel productivity in microalgal cultivation. Characterization studies confirm the

suitability of these nanoparticles for the effective conversion of microalgal lipids into biodiesel. Particularly, at 10 mg.L<sup>-1</sup> concentration, iron oxide nanoparticles significantly boost biomass concentration and growth rates in *Chlorella minutissima* cultures. The findings highlight the feasibility of integrating hematite nanoparticles into microalgal media for sustainable biofuel production.

## References

- Aghabeigi, F., Nikkhah, H., Zilouei, H., & Bazarganipour, M. (2023). Immobilization of lipase on the graphene oxides magnetized with NiFe<sub>2</sub>O<sub>4</sub> nanoparticles for biodiesel production from microalgae lipids. *Process Biochemistry*, 126, 171–185. <https://doi.org/10.1016/j.procbio.2023.01.012>
- Al-Ansari, M. M., Al-Humaid, L., Al-Dahmash, N. D., & Aldawsari, M. (2023). Assessing the benefits of *Chlorella vulgaris* microalgal biodiesel for internal combustion engines: Energy and exergy analyses. *Fuel*, 344, 128055. <https://doi.org/10.1016/j.fuel.2023.128055>
- Arif, M., Li, Y., El-Dalatony, M. M., Zhang, C., Li, X., & Salama, E.S. (2021). A complete characterization of microalgal biomass through FTIR/TGA/CHNS analysis: An approach for biofuel generation and nutrients removal. *Renewable Energy*, 163, 1973–1982. <https://doi.org/10.1016/j.renene.2020.10.066>
- Attre, T., Roy, A., & Bharadvaja, N. (2018). Influence of various Carbon and Nitrogen sources on Lipid productivity of *Chlorella minutissima* and *Scenedesmus* sp. and their FAME analysis. *Journal of Algal Biomass Utilization*, 9(1): 72–85. [https://doi.org/10.1016/0304-4157\(79\)90001-14](https://doi.org/10.1016/0304-4157(79)90001-14)
- Banerjee, S., Rout, S., Banerjee, S., Atta, A., & Das, D. (2019). Fe<sub>2</sub>O<sub>3</sub> nanocatalyst aided transesterification for biodiesel production from lipid-intact wet microalgal biomass: A biorefinery approach. *Energy Conversion and Management*, 195, 844–853. <https://doi.org/10.1016/j.enconman.2019.05.060>
- Bligh, E. G., & Dyer, W. J. (1959). A rapid method of total lipid extraction and purification. *Canadian Journal of Biochemistry and Physiology*, 37(8), 911–917. <https://doi.org/10.1139/o59-099>
- Boopathi, M., Sathiskumar, S., Manideep, B., Jayakrishnan, S., Praveen, S. B., Gokul, V., Sakthi Ganesh, P., & Gokulraj, V. (2023). Experimental investigation on performance and emission characteristics of algae oil biodiesel with methanol additive in CI engine. *Materials Today: Proceedings*, S2214785323014529. <https://doi.org/10.1016/j.matpr.2023.03.405>
- Chandra, R., Amit, & Ghosh, U. K. (2019). Effects of various abiotic factors on biomass growth and lipid yield of *Chlorella minutissima* for sustainable biodiesel production. *Environmental*

- Science and Pollution Research*, 26(4), 3848–3861. <https://doi.org/10.1007/s11356-018-3696-1>
- Cheng, J., Zhu, Y., Li, K., Lu, H., & Shi, Z. (2020). Calcinated MIL-100(Fe) as a CO<sub>2</sub> adsorbent to promote biomass productivity of *Arthrospira platensis* cells. *Science of the Total Environment*, 699, 134375. <https://doi.org/10.1016/j.scitotenv.2019.134375>
- Da Silva Vaz, B., Alberto Vieira Costa, J., & Greque De Morais, M. (2020). Physical and biological fixation of CO<sub>2</sub> with polymeric nanofibers in outdoor cultivations of *Chlorella fusca* LEB 111. *International Journal of Biological Macromolecules*, 151, 1332–1339. <https://doi.org/10.1016/j.ijbiomac.2019.10.179>
- Ganesh Saratale, R., Ponnusamy, V. K., Jeyakumar, R. B., Sirohi, R., Piechota, G., et al. (2022). Microalgae cultivation strategies using cost-effective nutrient sources: Recent updates and progress towards biofuel production. *Bioresource Technology*, 361, 127691. <https://doi.org/10.1016/j.biortech.2022.127691>
- Geng, L., Zhou, W., Qu, X., Sa, R., Liang, J., Wang, X., & Sun, M. (2023). Iodine values, peroxide values and acid values of Bohai algae oil compared with other oils during the cooking. *Heliyon*, 9(4), e15088. <https://doi.org/10.1016/j.heliyon.2023.e15088>
- Hassanpour, M., Hosseini Tafreshi, S. A., Amiri, O., Hamadani, M., & Salavati-Niasari, M. (2020). Toxic effects of Fe<sub>2</sub>WO<sub>6</sub> nanoparticles towards microalga *Dunaliella salina*: Sonochemical synthesis nanoparticles and investigate its impact on the growth. *Chemosphere*, 258, 127348. <https://doi.org/10.1016/j.chemosphere.2020.127348>
- He, M., Yan, Y., Pei, F., Wu, M., Gebreluel, T., Zou, S., & Wang, C. (2017). Improvement on lipid production by *Scenedesmus obliquus* triggered by low dose exposure to nanoparticles. *Scientific Reports*, 7(1), 15526. <https://doi.org/10.1038/s41598-017-15667-0>
- Huang, W., Zhou, Y., Zhao, T., Tan, L., & Wang, J. (2022). The effects of copper ions and copper nanomaterials on the output of amino acids from marine microalgae. *Environmental Science and Pollution Research*, 29(7), 9780–9791. <https://doi.org/10.1007/s11356-021-16347-3>
- Kadar, E., Rooks, P., Lakey, C., & White, D. A. (2012). The effect of engineered iron nanoparticles on growth and metabolic status of marine microalgae cultures. *Science of the Total Environment*, 439, 8–17. <https://doi.org/10.1016/j.scitotenv.2012.09.010>
- Kaliamurthi, S., Selvaraj, G., Cakmak, Z. E., Korkmaz, A. D., & Cakmak, T. (2019). The relationship between *Chlorella* sp. and zinc oxide nanoparticles: Changes in biochemical, oxygen evolution, and lipid production ability. *Process Biochemistry*, 85, 43–50. <https://doi.org/10.1016/j.procbio.2019.06.005>
- Kaushik, P., Garima, G., Abhishek Chauhan, A. C., & Pankaj Goyal, P. G. (2009). Screening of *Lyngbya majuscula* for potential antibacterial activity and HPTLC analysis of active methanolic extract. *Journal of Pure and Applied Microbiology*, 3 (1), 169–174.
- Khan, M. I., Shin, J. H., & Kim, J. D. (2018). The promising future of microalgae: Current status, challenges, and optimization of a sustainable and renewable industry for biofuels, feed, and other products. *Microbial Cell Factories*, 17(1), 36. <https://doi.org/10.1186/s12934-018-0879-x>
- Lassoued, A., Dkhil, B., Gadri, A., & Ammar, S. (2017). Control of the shape and size of iron oxide (A-Fe<sub>2</sub>O<sub>3</sub>) nanoparticles synthesized through the chemical precipitation method. *Results in Physics*, 7, 3007–3015. <https://doi.org/10.1016/j.rinp.2017.07.066>
- Lee, J.Y., Yoo, C., Jun, S.Y., Ahn, C.Y., & Oh, H.M. (2010). Comparison of several methods for effective lipid extraction from microalgae. *Bioresource Technology*, 101(1), S75–S77. <https://doi.org/10.1016/j.biortech.2009.03.058>
- Ma, X., Mi, Y., Zhao, C., & Wei, Q. (2022). A comprehensive review on carbon source effect of microalgae lipid accumulation for biofuel production. *Science of the Total Environment*, 806, 151387. <https://doi.org/10.1016/j.scitotenv.2021.151387>
- Mallick, N., Mandal, S., Singh, A. K., Bishai, M., & Dash, A. (2012). Green microalga *Chlorella vulgaris* as a potential feedstock for biodiesel. *Journal of Chemical Technology & Biotechnology*, 87(1), 137–145. <https://doi.org/10.1002/jctb.2694>
- Marsalek, B., Jancula, D., Marsalkova, E., Mashlan, M., Safarova, K., Tucek, J., & Zboril, R. (2012). Multimodal action and selective toxicity of zerovalent iron nanoparticles against cyanobacteria. *Environmental Science & Technology*, 46(4), 2316–2323. <https://doi.org/10.1021/es2031483>
- Mishra, S. R., Mohanty, M. K., Das, S. P., & Pattanaik, A. K. (2014). Optimization of base-catalyzed transesterification of *Simarouba glauca* oil for biodiesel production. *International Journal of Sustainable Energy*, 33(6), 1033–1040. <https://doi.org/10.1080/14786451.2013.796942>
- Mondal, M., Khan, A. A., & Halder, G. (2021). Estimation of biodiesel properties based on fatty acid profiles of *Chlamydomonas* sp. BTA 9032 and *Chlorella* sp. BTA 9031 obtained under mixotrophic cultivation conditions. *Biofuels*, 12(10), 1175–1181. <https://doi.org/10.1080/17597269.2019.1600453>
- Moschona, A., Spanou, A., Pavlidis, I. V., Karabelas, A. J., & Patsios, S. I. (2024). Optimization of Enzymatic Transesterification of Acid Oil for Biodiesel Production Using a Low-Cost Lipase: The Effect of Transesterification Conditions and

- the Synergy of Lipases with Different Regioselectivity. *Applied biochemistry and biotechnology*, 10.1007/s12010-024-04941-3.
- Muhammad, G., Alam, M. A., Mofijur, M., Jahirul, M. I., Lv, Y., Xiong, W., Ong, H. C., & Xu, J. (2021). Modern developmental aspects in the field of economical harvesting and biodiesel production from microalgae biomass. *Renewable and Sustainable Energy Reviews*, 135, 110209. <https://doi.org/10.1016/j.rser.2020.110209>
- Mykhaylenko, N. F., & Zolotareva, E. K. (2017). The effect of copper and selenium nanocarboxylates on biomass accumulation and photosynthetic energy transduction efficiency of the green algae *Clorella vulgaris*. *Nanoscale Research Letters*, 12(1), 147. <https://doi.org/10.1186/s11671-017-1914-2>
- Nematian, T., Salehi, Z., & Shakeri, A. (2020). Conversion of bio-oil extracted from *Chlorella vulgaris* micro algae to biodiesel via modified superparamagnetic nano-biocatalyst. *Renewable Energy*, 146, 1796–1804. <https://doi.org/10.1016/j.renene.2019.08.048>
- Pahariya, R., Chauhan, A., Ranjan, A., Basniwal, R. K., Upadhyay, S., Thakur, S. K., & Jindal, T. (2023). A critical review on the efficacy and mechanism of nanoparticle-based flocculants for biodiesel feedstock production from microalgae. *BioEnergy Research*, 17(2), 1065–1079. <https://doi.org/10.1007/s12155-023-10672-w>
- Paulson, E., & Jothibas, M. (2021). Significance of thermal interfacial in hematite (A-fe2o3) nanoparticles synthesized by sol-gel method and its characteristics properties. *Surfaces and Interfaces*, 26, 101432. <https://doi.org/10.1016/j.surfin.2021.101432>
- Porra, R. J., Thompson, W. A., & Kriedemann, P. E. (1989). Determination of accurate extinction coefficients and simultaneous equations for assaying chlorophylls a and b extracted with four different solvents: Verification of the concentration of chlorophyll standards by atomic absorption spectroscopy. *Biochimica et Biophysica Acta (BBA) - Bioenergetics*, 975(3), 384–394. [https://doi.org/10.1016/S0005-2728\(89\)80347-0](https://doi.org/10.1016/S0005-2728(89)80347-0)
- Portaccio, M., Famarzi, B., & Lepore, M. (2023). Probing biochemical differences in lipid components of human cells by means of atr-ftir spectroscopy. *Biophysica*, 3(3), 524–538. <https://doi.org/10.3390/biophysica3030035>
- Prabakaran, S., Manimaran, R., Mohanraj, T., & Ravikumar, M. (2021). Performance analysis and emission characteristics of VCR diesel engine fuelled with algae biodiesel blends. *Materials Today: Proceedings*, 45, 2784–2788. <https://doi.org/10.1016/j.matpr.2020.11.742>
- Qayoom, M., Shah, K. A., Pandit, A. H., Firdous, A., & Dar, G. N. (2020). Dielectric and electrical studies on iron oxide (A-fe2o3) nanoparticles synthesized by modified solution combustion reaction for microwave applications. *Journal of Electroceramics*, 45(1), 7–14. <https://doi.org/10.1007/s10832-020-00219-2>
- Rana, M. S., Bhushan, S., Sudhakar, D. R., & Prajapati, S. K. (2020). Effect of iron oxide nanoparticles on growth and biofuel potential of *Chlorella* spp. *Algal Research*, 49, 101942. <https://doi.org/10.1016/j.algal.2020.101942>
- Roy, B., Chandrasekaran, H., Palamadai Krishnan, S., Chandrasekaran, N., & Mukherjee, A. (2018). UVA pre-irradiation to P25 titanium dioxide nanoparticles enhanced its toxicity towards freshwater algae *Scenedesmus obliquus*. *Environmental Science and Pollution Research*, 25(17), 16729–16742. <https://doi.org/10.1007/s11356-018-1860-2>
- Saxena, P., Sangela, V., Ranjan, S., Dutta, V., Dasgupta, N., Phulwaria, M., Rathore, D. S., & Harish. (2020). Aquatic nanotoxicology: Impact of carbon nanomaterials on algal flora. *Energy, Ecology and Environment*, 5(4), 240–252. <https://doi.org/10.1007/s40974-020-00151-9>
- Shi, K., Gao, Z., Shi, T. Q., Song, P., Ren, L. J., Huang, H., & Ji, X. J. (2017). Reactive oxygen species-mediated cellular stress response and lipid accumulation in oleaginous microorganisms: the state of the art and future perspectives. *Frontiers in microbiology*, 8, 793.
- Sun, YP, Li, X., Cao, J., Zhang, W., & Wang, H. P. (2006). Characterization of zero-valent iron nanoparticles. *Advances in Colloid and Interface Science*, 120(1–3), 47–56. <https://doi.org/10.1016/j.cis.2006.03.001>
- Taghizadeh, S. M., Ebrahiminezhad, A., Raei, M. J., Ramezani, H., Berenjian, A., & Ghasemi, Y. (2022). A study of l-lysine-stabilized iron oxide nanoparticles (IONPs) on microalgae biofilm formation of *Chlorella vulgaris*. *Molecular Biotechnology*, 64(6), 702–710.
- Tesfa, B., Mishra, R., Zhang, C., Gu, F., & Ball, A. D. (2013). Combustion and performance characteristics of CI (Compression ignition) engine running with biodiesel. *Energy*, 51, 101–115. <https://doi.org/10.1016/j.energy.2013.01.010>
- Thirugnanasambandham, K. (2018). Biodiesel production from *Chlorella minutissima* microalgae: Kinetic and mathematical modeling. *Energy Sources, Part A: Recovery, Utilization, and Environmental Effects*, 40(12), 1461–1468. <https://doi.org/10.1080/15567036.2018.1477872>
- Vasistha, S., Khanra, A., Clifford, M., & Rai, M. P. (2021). Current advances in microalgae harvesting and lipid extraction processes

- for improved biodiesel production: A review. *Renewable and Sustainable Energy Reviews*, 137, 110498. <https://doi.org/10.1016/j.rser.2020.110498>
- Wallach, D. F. H., Verma, S. P., & Fookson, J. (1979). Application of laser raman and infrared spectroscopy to the analysis of Membrane structure. *Biochimica et Biophysica Acta (BBA) - Reviews on Biomembranes*, 559(2–3), 153–208. [https://doi.org/10.1016/0304-4157\(79\)90001-7](https://doi.org/10.1016/0304-4157(79)90001-7)
- Wang, F., Liu, T., Guan, W., Xu, L., Huo, S., Ma, A., Zhuang, G., & Terry, N. (2021). Development of a strategy for enhancing the biomass growth and lipid accumulation of *Chlorella* sp. Uj-3 using magnetic fe<sub>3</sub>o<sub>4</sub> nanoparticles. *Nanomaterials*, 11(11), 2802. <https://doi.org/10.3390/nano11112802>
- Yaşar, F. (2020). Comparison of fuel properties of biodiesel fuels produced from different oils to determine the most suitable feedstock type. *Fuel*, 264, 116817.
- Zhao, Q., Han, F., You, Z., Huang, Y., She, X., Shi, X., & Han, P. (2024a). Evaluation of microalgae biodiesel for carbon neutrality based on the waste treatment by the autotrophic and heterotrophic combination. *Energy*, 291, 130314.
- Zhao, Y., Chen, Z., Li, W., Liu, F., Sun, L., Wu, M., Zhang, P., Hou, L., Li, M., & Xu, J. (2024b). Revealing the molecular basis regulating the iron deficiency response in quinoa seedlings by physio-biochemical and gene expression profiling analyses. *Plant and Soil*, 495(1–2), 77–97. <https://doi.org/10.1007/s11104-023-06094-4>